Interferometric synthetic aperture microscopy

P. Scott Carney, Brynmor J. Davis, Tyler S. Ralston, Daniel L. Marks, and Stephen A. Boppart

Beckman Institute for Advanced Science and Technology, Department of Electrical and Computer Engineering,

University of Illinois at Urbana-Champaign, 405 North Mathews Avenue, Urbana, Illinois 61801

Interferometric synthetic aperture microscopy provides high-resolution three-dimensional optical images of semitransparent samples with large depth of field without scanning the focal plane. ISAM theory and experiments will be discussed.

OCIS codes: 100.3190, 100.6890, 170.1650, 170.4500, 110.6880, 180.3170

Optical coherence tomography (OCT) is a powerful modality for optical and near-infrared three-dimensional imaging in medicine and biology [1–4]. Interferometric synthetic aperture microscopy (ISAM) is a recently developed modality based on a solution of the inverse scattering problem for instrumentation similar to OCT with augmentation to provide phase stability over the data set. ISAM has been demonstrated in simulation [5–9] and in experiments with tissue phantoms and human tissue [10]. It offers advantages over OCT in that it is quantitative and that images may be obtained over many confocal lengths in the axial direction without scanning the focus. Thus there is no need to compromise between depth of field and resolution as there is in OCT.

The physical models for light scattering and the mathematics of ISAM are presented. It will be seen that the mathematical expressions for the ISAM signal are amenable to two different asymptotic treatments that happen to result in identical resampling schemes for double-pass instruments, the modality currently practiced. This resampling scheme leads to fast algorithms for data processing to provide computed reconstructions of the sample in three dimensions with uniform resolution. Thus ISAM provides a means to bring into focus data from regions that appear out-of-focus in OCT. The many advantages of this method are discussed including some less obvious benefits such as a mitigation of the effects of autocorrelation in the interferometric signal. Experimental results are presented and future directions discussed.

In OCT and ISAM, a beam of light is projected into a semitransparent sample and the back-scattered light is collected and measured in an interferometer. The center of the beam in a plane perpendicular to the beam axis is denoted by a position vector that labels each set of data or so-called axial scan. At each position of the beam, data are collected interferometrically as a function of frequency, ω, either directly or by Fourier transform from the time domain. The data may then be written as a function of position and wavenumber, $k = n(\omega)\omega/c$, where $n(\omega)$ denotes a generally dispersive effective background index of refraction [11]. In OCT, the data from distinct axial scans are treated as independent and an image is obtained by taking the one-dimensional inverse Fourier transform with respect to k. ISAM takes into account a more complete model that includes scattering and beam diffraction effects. Data in different axial scans are related and it becomes vital to establish phase stability between scans. It may be seen that the interferometric signal is related to object susceptibility, η by the relation [7]

$$S(\mathbf{r_0}, k) = A(k) \int_{z=0} \mathrm{d}^2 r \int \mathrm{d}^3 r' G(\mathbf{r}', \mathbf{r}, k) g(\mathbf{r}' - \mathbf{r}_0, k) g(\mathbf{r} - \mathbf{r}_0, k) \eta(\mathbf{r}') \tag{1}$$

where g describes the aperture function of the system and G is the green function. Within the scalar model for the field emerging from a single-mode fiber, g is usually well-approximated by a Gaussian.

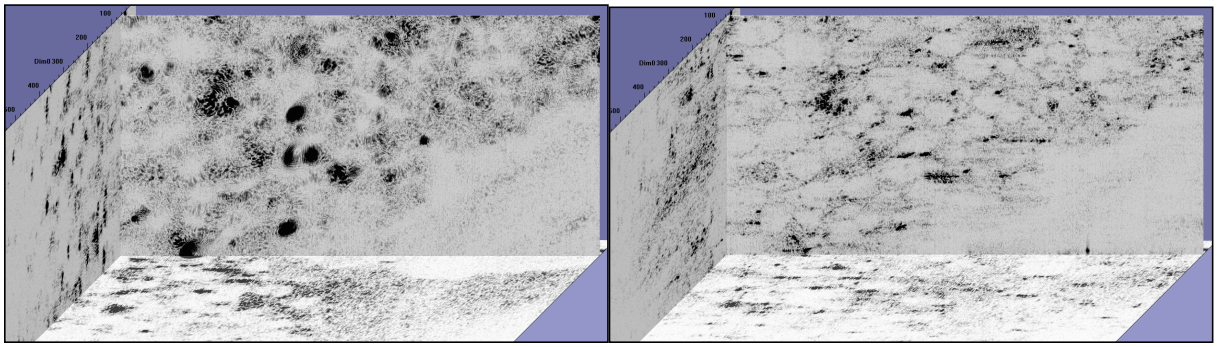

Fig. 1. An *en face* OCT image of human breast tissue 4.9 Rayleigh ranges from the focal plane (left) and an ISAM image of human breast tissue 4.9 Rayleigh ranges from the focal plane (right). Here a Rayleigh range is 120μm and the *en face* images are 720μm $\times$ 360μm.

The relationship between the signal and the sample structure expressed in Eq. (1) is linear and may thus be inverted by standard computational methods. However, it should be understood that the numerical inversion of an integral equation in three dimensions will necessarily be very computationally expensive *i.e.* slow. A careful analysis reveals that the expression simplifies significantly in at least two asymptotic regimes [9]. The first corresponds to the signal originating from points in and near the confocal region. The large expansion parameter may be taken to be π/NA and the resultant expansion is seen to be dominated by the leading term even as $NA \to 1$. The second regime corresponds to signals originating far from the aperture plane. A stationary phase expansion of the integral yields a series of ray approximations, the first term being the direct ray, the next the so-called boundary ray, *etc.* Taking the two-dimensional Fourier transform of S (indicated by a tilde) with respect to $\mathbf{r}_0$, and using the asymptotic methods described above [7, 9], it may be found that in both regimes

$$\tilde{S}(\mathbf{Q}, k) = K(\mathbf{Q}, k)\tilde{\tilde{\eta}}\left[\mathbf{Q}, -2\sqrt{k^2 - Q^2/4}\right], \tag{2}$$

where $\tilde{\tilde{\eta}}$ is the three-dimensional Fourier transform of the susceptibility and describes the structure of the sample. The object structure may then be recovered by filtering and resampling in the Fourier domain followed by a three-dimensional inverse Fourier transform. Since the relationship between the data and the object structure is, to a good approximation, expressible entirely in the Fourier domain, there is necessarily no preferred location. The resolution is thus expected to be spatially uniform and everywhere equal to the resolution of the raw data in the focal plane.

Results of ISAM imaging are shown in Fig. (1) and compared to OCT data outside the confocal region. The details of the experimental implementation may be found elsewhere [10]. A key step in implementation is the stabilization of the instrument to ensure phase coherence across the entire data set. In each axial scan, the signal must be dispersion compensated [11]. Data acquisition and processing time is under one-half second per frame for frame sizes of 512 $\times$ 1024 pixels.

ISAM obviously provides certain advantages over OCT in that the focus need not be scanned and there is no trade between depth of imaging and resolution. These benefits allow the design of mechanically simpler instrumentation with superior resolution (as compared to OCT) expected therefore to be more robust and amenable to use in a clinical setting. Several other benefits obtain. ISAM reconstructions are quantitatively meaningful and therefore may have greater diagnostic value. The problem of image artifacts associated with the autocorrelation in spectral domain instruments is seen to be mitigated by ISAM reconstruction [12]. That is, the computational focusing of the

expected signal has the effect of defocusing the signal associated with the unwanted autocorrelation. A theoretical analysis and experimental demonstration of this effect are presented.

References

1. D. Huang, E. A. Swanson, C. P. Lin, W. G. Stinson, W. Chang, R. Hee, T. Flotte, K. Gregory, C. A. Puliafito, and J. G. Fujimoto, "Optical coherence tomography," Science **254**, 1178–1181 (1991).
2. G. J. Tearney, M. E. Brezinski, B. E. Bouma, S. A. Boppart, C. Pitris, J. F. Southern, and J. G. Fujimoto, "In Vivo Endoscopic Optical Biopsy with Optical Coherence Tomography," Science **276**, 2037–2039 (1997).
3. S. A. Boppart, B. E. Bouma, C. Pitris, G. J. Tearney, J. F. Southern, M. E. Brezinski, and J. G. Fujimoto, "Intraoperative assessment of microsurgery with three-dimensional optical coherence tomography," Radiology **208**, 81–86 (1998).
4. M. E. Brezinski, G. J. Tearney, B. Bouma, S. A. Boppart, C. Pitris, and J. G. Fujimoto, "Optical biopsy with optical coherence tomography," Ann. NY Acad. Sci. **838**, 68–74 (1998).
5. T. Ralston, D. L. Marks, P. S. Carney, and S. A. Boppart, "Inverse scattering for interferometric synthetic aperture microscopy," Journ. Opt. Soc. Am. A **23**, 1027–1037 (2006).
6. D. L. Marks, T. S. Ralston, P. S. Carney, and S. A. Boppart, "Inverse scattering for rotationally-scanned optical coherence tomography," Journ. Opt. Soc. Am. A *in press* (2006).
7. T. S. Ralston, D. L. Marks, S. A. Boppart, and P. S. Carney, "Inverse scattering for high-resolution interferometric microscopy," Opt. Lett. **31**, 3585–3587 (2006).
8. D. L. Marks, T. S. Ralston, P. S. Carney, and S. A. Boppart, "Inverse scattering for frequency-scanned full-field optical coherence tomography," J. Opt. Soc. Am. A **in press** (2007).
9. B. J. Davis, S. C. Schlachter, D. L. Marks, T. S. Ralston, S. A. Boppart, and P. S. Carney, "Non-paraxial vector-field modeling of optical coherence tomography and interferometric synthetic aperture microscopy," (submitted) (2006).
10. T. S. Ralston, D. L. Marks, P. S. Carney, and S. A. Boppart, "Interferometric Synthetic Aperture Microscopy," Nat. Phys. **3**, 129–134 (2007).
11. D. L. Marks, A. L. Oldenburg, J. J. Reynolds, and S. A. Boppart, "A digital algorithm for dispersion correction in optical coherence tomography," Appl. Opt. **42**, 204–217 (2003).
12. B. J. Davis, D. L. Marks, T. S. Ralston, S. A. Boppart, and P. S. Carney, "Autocorrelation artifacts in optical coherence tomography and interferometric synthetic aperture microscopy," (submitted) (2006).